Possible Novel Mn^{1+} oxidation states in infinite-layer La_2MnRhO_{6-x}

1 Computational Details

Theoretical calculations are performed based on first-principles density functional theory (DFT) method with the PBE generalized gradient approximation (GGA) implemented in Vienna ab initio Simulation Package (VASP). The strong-correlated correction is considered with GGA+U method. The effective onsite Coulomb interaction parameter U_{eff} is set to be 4 for Mn and 3 for Rh.

A $11 \times 11 \times 11$ k-point grid is used for geometry optimization with fixed volume, while a $15 \times 15 \times 15$ grid is generally used for calculating Density of States. A $2 \times 2 \times 2$ supercell is used for calculating magnetic coupling constants. Maximum allowed error in energy is set as 10^{-4} eV.

U_{eff} values are extracted from [1]. Test calculations are carried out for La_2MnRhO_6, predicting a=b=5.62Å, c=3.90Å against experimental values of a=b=5.60Å, c=3.92Å[2], and $LaRhO_3$, predicting a=5.46Å, b=5.74Å, c=7.84Å against experimental values of a=5.52Å, b=5.70Å, c=7.80Å[3].

2 Results and Discussion

2.1 Geometry

Lattice parameters are found to depend significantly on O stoichiometry (Figure 1), slightly on U_{eff} (Figure 1) as well as alignment of Mn and Rh atoms, and on hydrogenation (Figure 2). They are also strongly dependent on doping concentration of Mn (Figure 3). The predicted lattice constants suggest that the x value in La_2MnRhO_{6-x} is between 1 and 2. However, no definite conclusion on the chemical composition of the synthesized perovskite can be reliably drawn.

No distortion of O lattice or asymmetry of charge distribution is predicted for La_2MnRhO_4.

2.2 Electronic Structure

The valence states of $La_2MnRhO_{4.5}$ is a conventional $La_2^{3+}Mn^{2+}Rh^{1+}O_{4.5}^{2-}$. There is no d electron in La or $d_\downarrow$ electron in Mn (Figure 4), and the $4.36\mu_B$ magnetization of Mn also suggests a high-spin d^5 configuration.

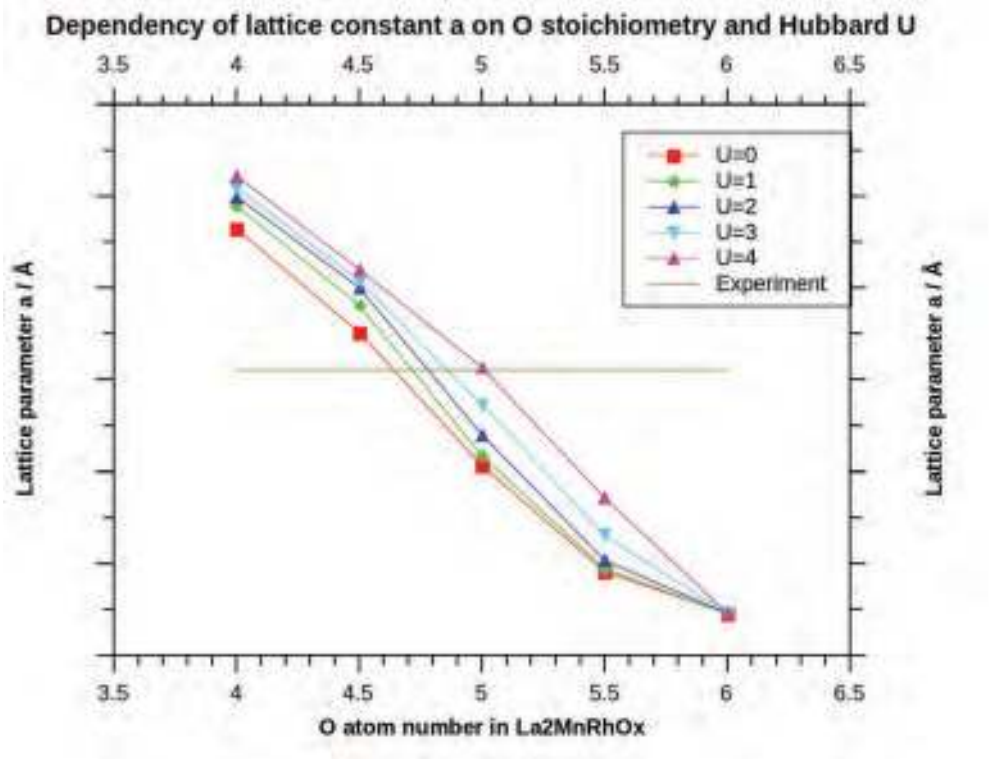

Figure 1: Dependency of lattice constant a on O stoichiometry and U_{eff}

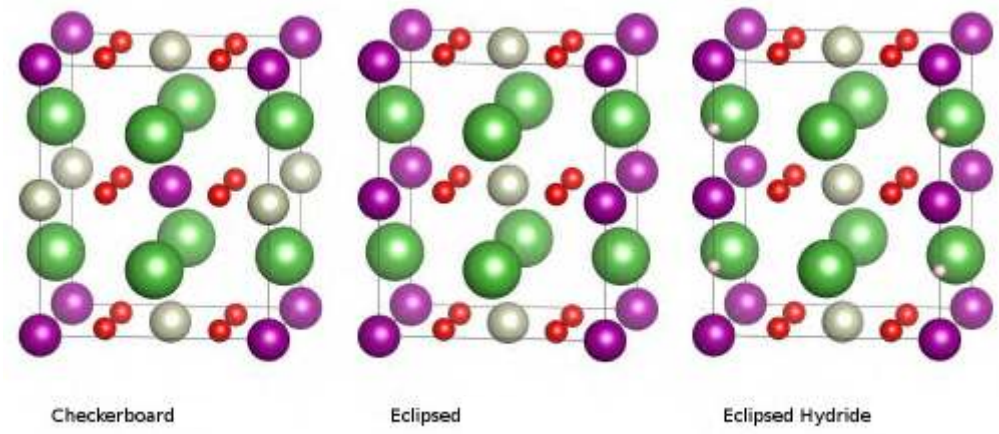

Figure 2: Lattice constant a in checkerboard, eclipsed and eclipsed hydride structures

Orbital energies are ordered based on position of DOS peaks. lm-projected DOS is integrated up to Fermi level to determine orbital occupancy, and the result is summarized in Table 1. The electronic configuration for Mn is $d^1_{z^2}d^1_{xz}d^1_{yz}d^1_{xy}d^1_{x^2-y^2}$, and that of

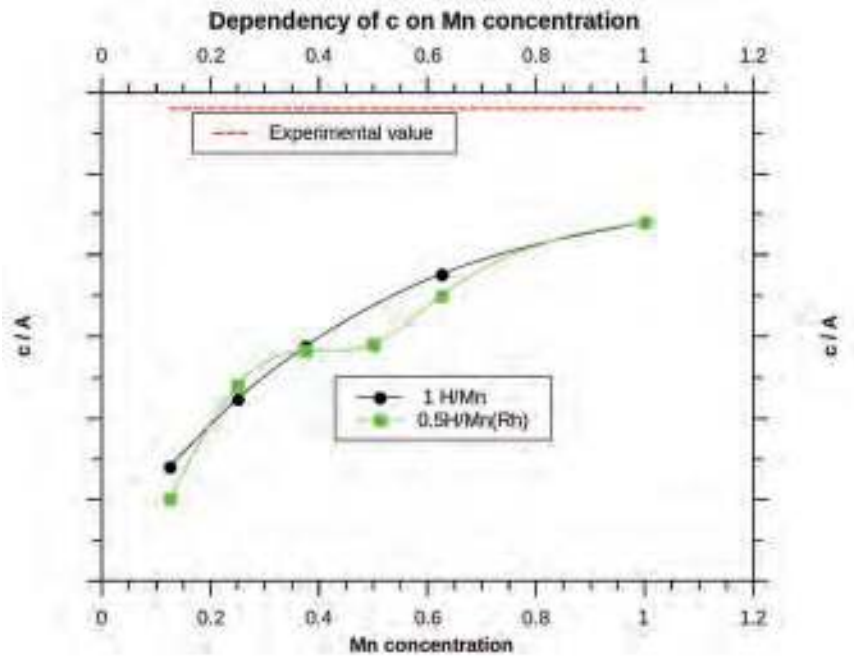

Figure 3: Dependency of lattice constant c on Mn doping ratio

Rh is $d_{z^2}^2 d_{xz}^2 d_{yz}^2 d_{xy}^2$, shown schematically in Figure 5. In short, electronic configurations are conventional.

$Mn_\uparrow$	s 0.14 p_y 0.06 p_z 0.07 p_x 0.06 d_{yz} 0.97 d_{xy} 0.94 d_{z^2} 0.84 d_{xz} 0.93 $d_{x^2-y^2}$ 0.94
$Mn_\downarrow$	s 0.12 p_y 0.05 p_z 0.05 p_x 0.05 d_{yz} 0.10 d_{xy} 0.04 d_{z^2} 0.13 d_{xz} 0.04 $d_{x^2-y^2}$ 0.04
$Rh_\uparrow$	s 0.16 p_y 0.07 p_z 0.05 p_x 0.07 d_{yz} 0.40 d_{xy} 0.89 d_{z^2} 0.55 d_{xz} 0.87 $d_{x^2-y^2}$ 0.91
$Rh_\downarrow$	s 0.16 p_y 0.07 p_z 0.07 p_x 0.07 d_{yz} 0.31 d_{xy} 0.88 d_{z^2} 0.61 d_{xz} 0.86 $d_{x^2-y^2}$ 0.90
$La_\uparrow$	s 1.00 p_y 0.95 p_z 0.95 p_x 0.95 d_{yz} 0.03 d_{xy} 0.04 d_{z^2} 0.03 d_{xz} 0.04 $d_{x^2-y^2}$ 0.03
$La_\downarrow$	s 1.00 p_y 0.95 p_z 0.95 p_x 0.95 d_{yz} 0.03 d_{xy} 0.04 d_{z^2} 0.03 d_{xz} 0.04 $d_{x^2-y^2}$ 0.03

Table 1: Partial orbital occupancies

Electronic structures of La_2MnRhO_{6-x} ($x = 0, 0.5, 1, 1.5, 2$) are compared. Every time an O atom is inserted between a Mn and a Rh atom, both Mn and Rh get half an electron (Bader charge, Figure 6). On the other hand, orbital occupation integrated inside Wigner-Seitz radius stays around that of $La_2MnRhO_{4.5}$ described above, with a decrement less than 0.3 per orbital from La_2MnRhO_4 to La_2MnRhO_6 (Wigner-Seitz charge, Figure 6). Based on the fact that the Bader charge analysis covers more interatomic space than the RWIGS charge and includes more bonding electrons, the charge transfer process could be generalized as electrons sticking to a happy configuration in the vicinity of the nuclei while leaving the extra electrons to the bonding regions.

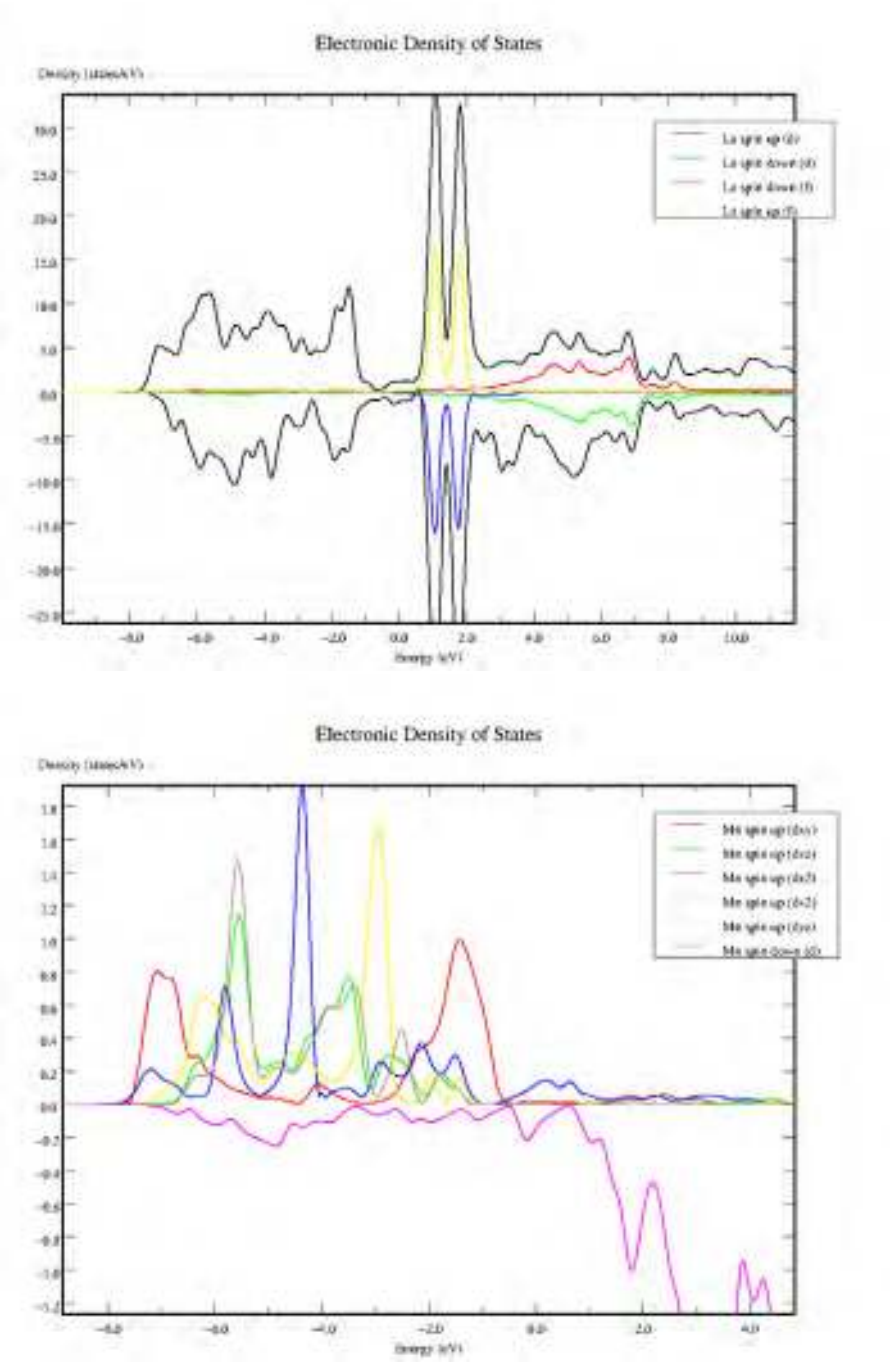

Figure 4: lm-projected DOS of La d and Mn d orbital

La_2MnRhO_{6-x} is predicted to be a conductor for $0 \leq x \leq 2$.

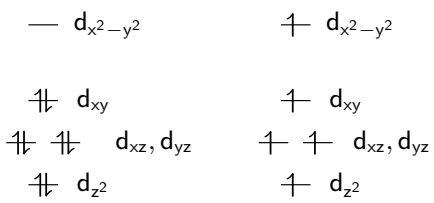

Figure 5: Orbital configuration of Mn(right) and Rh(left)

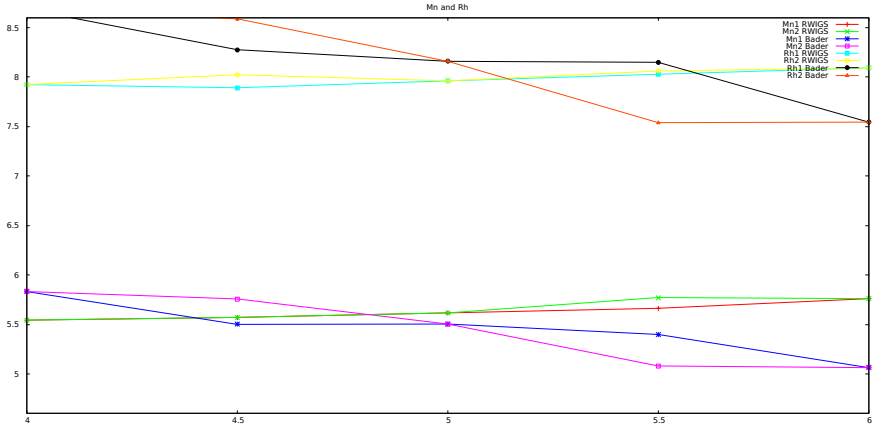

Figure 6: Charge transfer in oxidizing process

2.3 Magnetic Coupling

Computations are performed for 9 different spin configurations to obtain magnetic coupling constants (see Figure 8). Based on the Heisenberg Hamiltonian $H = \sum_{i<j} J_{ij} S_i S_j$ with $S = \pm 2.5$, the relationship between energy and spins can be expressed as follows:

$$
\begin{aligned}
E &= E_0 + \begin{pmatrix} S_1 & S_2 & \cdots & S_n \end{pmatrix} \begin{pmatrix} C_{11} & C_{12} & \dots & C_{1n} \\ C_{21} & C_{22} & \dots & C_{2n} \\ \vdots & \vdots & \vdots & \vdots \\ C_{n1} & C_{n2} & \dots & C_{nn} \end{pmatrix} \begin{pmatrix} S_1 \\ S_2 \\ \vdots \\ S_n \end{pmatrix} \\
&= E_0 + \sum_i J_i \cdot \overrightarrow{S} \overleftrightarrow{A_i} \overrightarrow{S}^T
\end{aligned}
$$

where $(A_i)_{jk} = 1 \iff C_{jk} = J_i$. An equation array for variables J_i and E_0 is constructed and solved with the linear least square method implemented in NumPy. Magnetic interactions are classified into 4 types of J's by interatomic distances (Figure

7). The corresponding equation array is

$$\begin{cases} -75.0J_1 + 100.0J_2 + 0.0J_3 + 100.0J_4 + 1.0J_5 & = -970.980958\text{eV} \\ 0.0J_1 + -200.0J_2 + -100.0J_3 + 200.0J_4 + 1.0J_5 & = -970.220796\text{eV} \\ 0.0J_1 + -200.0J_2 + 100.0J_3 + 200.0J_4 + 1.0J_5 & = -970.232559\text{eV} \\ 0.0J_1 + 0.0J_2 + 100.0J_3 + -200.0J_4 + 1.0J_5 & = -970.142065\text{eV} \\ 0.0J_1 + 200.0J_2 + -100.0J_3 + 200.0J_4 + 1.0J_5 & = -971.212904\text{eV} \\ 0.0J_1 + 200.0J_2 + -100.0J_3 + 200.0J_4 + 1.0J_5 & = -971.212905\text{eV} \\ -400.0J_1 + 200.0J_2 + 100.0J_3 + 200.0J_4 + 1.0J_5 & = -971.272466\text{eV} \\ 100.0J_1 + 100.0J_2 + 0.0J_3 + 0.0J_4 + 1.0J_5 + & = -970.728227\text{eV} \\ 400.0J_1 + 200.0J_2 + 100.0J_3 + 200.0J_4 + 1.0J_5 + & = -971.267781\text{eV} \end{cases}$$

Calculated J and E_0 values are summarised in Table 2. It was also observed that magnetic moment of Rh, though small, automatically aligns with that of majority Mn in the self-consistent process.

J_1/cm^{-1}	J_2/cm^{-1}	J_3/cm^{-1}	J_4/cm^{-1}	E_0/eV
0.23	-20.73	-1.18	-11.74	-970.5

Table 2: Calculated values of exchange parameter J

From the table, it could be concluded that magnetic coupling between Mn atoms are weak except for a ferromagnetic coupling in the diagonal and lateral directions in the Mn-Rh-O plane. Along the diagonal direction, atoms align in a Mn-O-Rh-O-Mn pattern. It may be accounted for by a strong ferromagnetic coupling between Mn and Rh, which is in line with the observation that the total spin of Rh automatically aligns with that of Mn, and which may in turn be explained by double exchange.

Among the 9 configurations calculated, the layered antiferromagnetic configuration (5th of Figure 8) is energetically most favorable.

It is also found that although the interplanar interaction of La_2MnRhO_4 is antiferromagnetic, that of La_2MnRhO_6 is ferromagnetic(Figure 9). The antiferromagnetic interplanar coupling also vanishes if Hubbard U is removed (Figure 10).

3 Summary

Geometry of the unit cell depend strongly on x value for La_2MnRhO_{6-x}, and it is unclear whether it is 4 or 4.5. The O-stiochiometry, however, has little impact on electron distribution within the Wigner-Seitz radius, which resembles the electronic configuration of canonical $La_2MnRhO_{4.5}$, whereas the rest of the charge resides in interatomic regions. Magnetic coupling for La_2MnRhO_{6-x} transitions from (weak) AFM to FM as x decreases to 0.

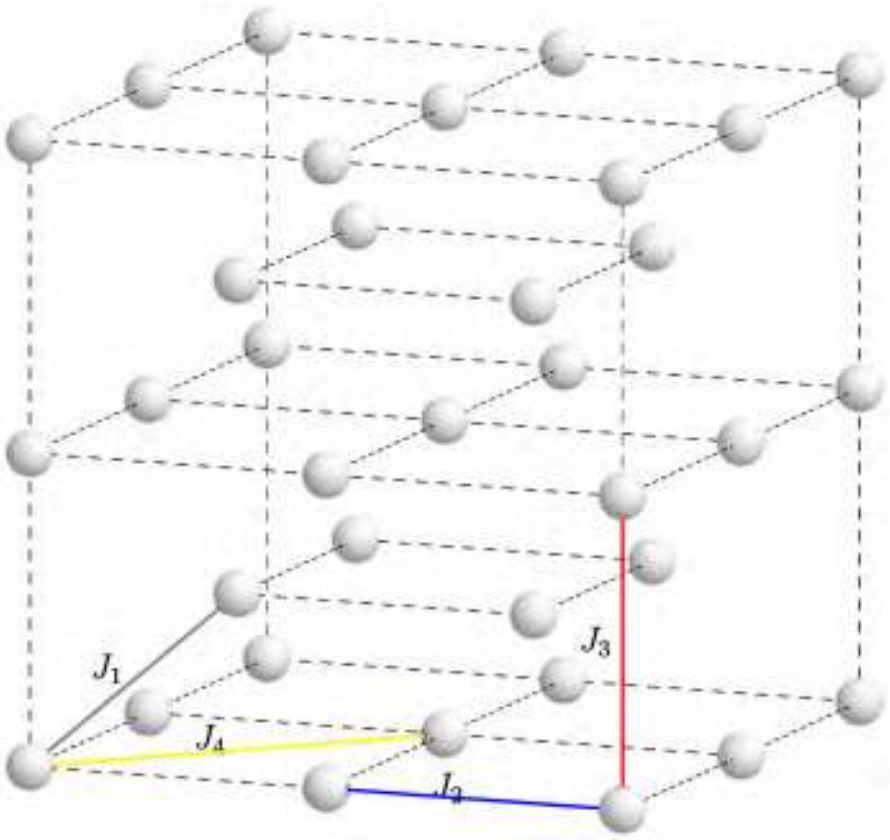

Figure 7: Definition of J_1, J_2, J_3, J_4

References

[1] IV Solovyev, PH Dederichs, and VI Anisimov. Corrected atomic limit in the local-density approximation and the electronic structure of d impurities in rb. *Physical Review B*, 50(23):16861, 1994.

[2] C Schinzer. A new ferromagnetic perovskite: Lamn 1/2 rh 1/2 o 3. *Journal of Physics and Chemistry of Solids*, 61(10):1543–1551, 2000.

[3] René B Macquart, Mark D Smith, and Hans-Conrad zur Loye. Crystal growth and single-crystal structures of re rho3 (re= la, pr, nd, sm, eu, tb) orthorhodites from a k2co3 flux. *Crystal growth & design*, 6(6):1361–1365, 2006.

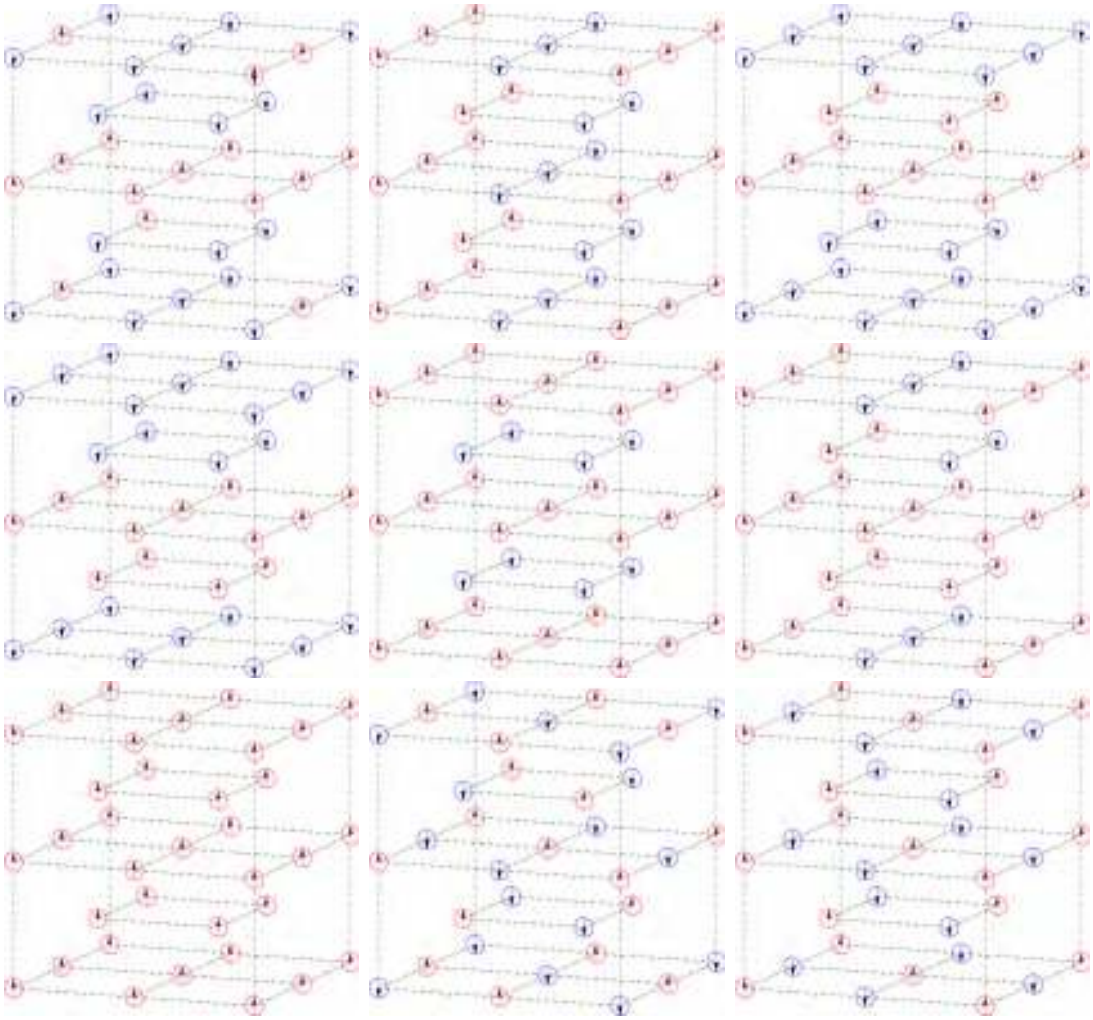

Figure 8: Spin configurations for calculating magnetic coupling constant

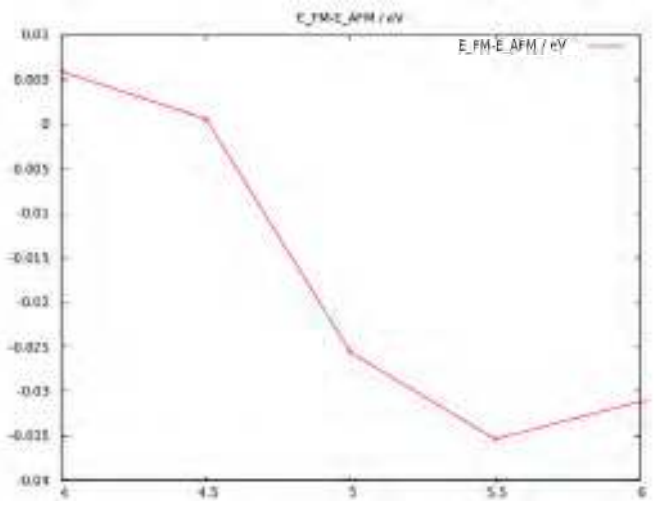

Figure 9: $E_{FM}-E_{AFM}$ for LDA+U calculations

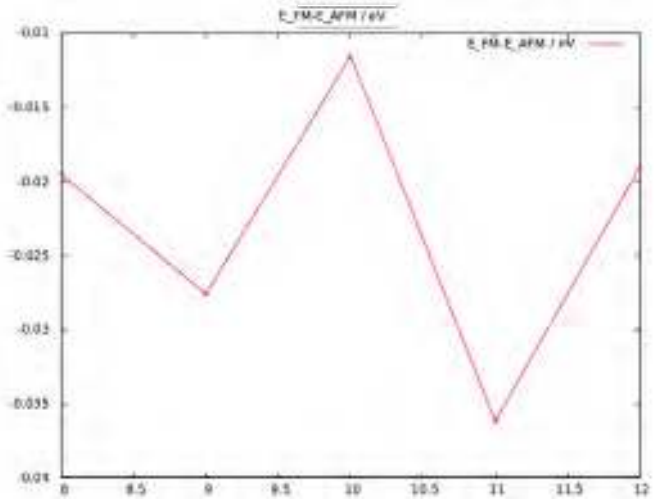

Figure 10: $E_{FM}-E_{AFM}$ for LDA calculations